Lithium motion in the anode material LiC_6 as seen via time-domain ^{7}Li NMR

J. Langer,[1,*] V. Epp,[1,†] P. Heitjans,[2] F. A. Mautner,[1] and M. Wilkening[1,‡]

[1]*Christian Doppler Laboratory for Lithium Batteries, and Institute for Chemistry and Technology of Materials, Graz University of Technology, Stremayrgasse 9, 8010 Graz, Austria*

[2]*Institute of Physical Chemistry and Electrochemistry, Leibniz University Hannover, Callinstraße 3-3a, 30167 Hannover, Germany*

(Received 28 June 2013; revised manuscript received 28 August 2013; published 16 September 2013)

Since the commercialization of rechargeable lithium-ion energy storage systems in the early 1990s, graphite intercalation compounds (GICs) have served as the number one negative electrode material in most of today's batteries. During charging the performance of a battery is closely tied with facile Li insertion into the graphite host structure. So far, only occasionally time-domain nuclear magnetic resonance (NMR) measurements have been reported to study Li self-diffusion parameters in GICs. Here, we used several NMR techniques to enlighten Li hopping motions from an atomic-scale point of view. Li self-diffusion in the stage-1 GIC LiC_6 has been studied comparatively by temperature-variable spin-spin relaxation NMR as well as (rotating frame) spin-lattice relaxation NMR. The data collected yield information on both the relevant activation energies and jump rates, which can directly be transformed into Li self-diffusion coefficients. At room temperature the Li self-diffusion coefficient turns out to be 10^{-15} m^2 s^{-1}, thus, slightly lower than that for layer-structured cathode materials such as $Li_{x\approx 0.7}TiS_2$.

DOI: 10.1103/PhysRevB.88.094304 PACS number(s): 66.30.−h, 76.60.−k, 82.56.−b

I. INTRODUCTION

The stage-1 graphite intercalation compound, LiC_6, belongs to one of the most fascinating application-oriented materials which is widely used as an anode in secondary lithium-ion batteries.[1–3] Most of the various electronic devices of our daily life such as notebooks or cell phones rely on the insertion and deinsertion of lithium ions into graphite-based negative electrodes.[4] In particular, the charge/discharge performance and thus the rate capability of an anode is closely related to self-diffusion of lithium ions inside the crystalline host. Moreover, if models are to succeed in simulation of the electrochemical processes in batteries, precisely measured data such as diffusion parameters are required.

Surprisingly, only a few studies can be found in the literature which directly deal with the in-depth investigation of Li diffusion parameters in crystalline, phase-pure LiC_6. Despite the relatively simple, but fascinating, structure of LiC_6 research is yet far away from drawing a comprehensive picture on diffusive Li motion. Apart from earlier studies[5] applying quasielastic neutron scattering (QENS)[6] or taking advantage of β-radiation detected nuclear magnetic resonance (β-NMR) measurements of spin-polarized ^{8}Li ($t_{1/2} = 0.8$ s) nuclei produced *in situ* by polarized neutron capture,[7–9] classical NMR measurements[9–13] on the stable Li isotope ^{7}Li have rarely been utilized for this purpose. *En passant*, the results obtained from ^{7}Li pulsed NMR as yet turned out to be less conclusive with respect to Li diffusion parameters.[14] This is because mainly spin-lattice relaxation (SLR) measurements in the so-called laboratory frame of reference have been performed. Compared to other time-domain NMR techniques, those measurements are sensitive to Li jump rates with values in the MHz range.[10] However, in order to probe Li motional processes in the temperature range where the structurally ordered LiC_6 phase does exist, i.e., at ambient temperature, alternative NMR techniques have to be applied which are able to access much slower Li motions. For example, this is possible by recording SLR rates R_1 in the rotating (ϱ) frame of reference via the so-called spin-lock technique introduced by Ailion and Slichter.[11,13,15–18] If ^{7}Li SLR takes solely place in the presence of a controllable magnetic field with resonance frequencies on the order of a few kHz instead of some MHz,[19] the desirable diffusion-induced rate peak $R_1(1/T)$ shows up at much lower temperatures T.[11,18] In general, the peak entails valuable information on both short-range and long-range motions[9,13,18] as well as correlation effects.[20,21]

Here, layer-structured LiC_6 (see Fig. 1) served as an excellent model system to probe Li dynamics with spatially confined migration pathways; it is the most prominent anode host material with applications in energy storage technology. The stage-1 compound consists of commensurate layers of carbon and lithium; Li resides in the central site below and above each third hexagon formed by C atoms. The stacking sequence is AαAα with a periodicity of 3.71 Å; A denotes the graphite basal plane and α the intercalate layer. The carbon host structure of LiC_6 allows in-plane jump diffusion and, because of the open channels parallel to the hexagonal c

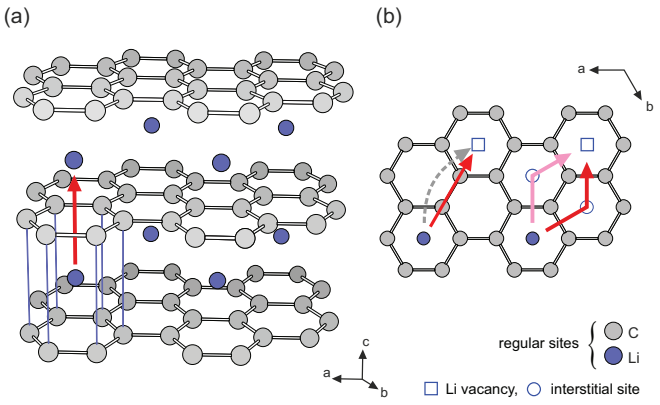

FIG. 1. (Color online) Illustration of the crystal structure of ordered LiC_6 with AαAα stacking sequence. (a) View along the ab plane; (b) view along the c axis. Arrows roughly indicate possible Li^+ migration pathways, that is, in-plane diffusion (b) vs motion along the open channels parallel to the hexagonal axis (a). A detailed description of possible migration pathways can be found in Ref. 22.

axis and the small size of the Li ion, it has been argued that also diffusion normal to the graphite plane cannot be ruled out *a priori* as in the case of the heavy alkalis.[23] In the present contribution, the results from various ^{7}Li NMR measurements investigating both (local electronic) structure and Li ion dynamics of polycrystalline LiC_6 will be presented and compared with those deduced from previous β-NMR[7,8] and QENS studies,[5] in particular. While β-NMR results were obtained on highly oriented pyrolytic graphite (HOPG) at temperatures around 373 K, results from QENS being sensitive to Li correlation times in the ns to ps range, were collected at much higher T, i.e., in a range with sufficiently fast Li motion.

II. EXPERIMENT

The synthesis procedure to obtain polycrystalline stage-1 LiC_6, shining like gold, is described in the classical paper by Guérard and Hérold.[24] After preparation, the sample (approximately 300 mg) was sealed in a quartz ampoule (3 cm in length, 5 mm in diameter) and stored for several months at room temperature; we anticipate almost full lithium homogenization, i.e., a homogenous distribution of the Li ions between the layers. The sample consists of LiC_6 crystallites with diameters less than 500 μm. Phase purity was checked by x-ray powder diffraction (XRPD). XRPD revealed a small volume fraction of the stage-2 compound LiC_{12} formed. By NMR, however, it was very difficult to detect this minor phase (see below and Fig. 2). The same sample was used for all measurements presented below.

^{7}Li NMR measurements were carried out using two different high-performance digital Bruker Avance III spectrometers in connection with shimmed cryomagnets with nominal magnetic fields of 7 T and 11 T, respectively. This corresponds to ^{7}Li Larmor frequencies of $\omega_0/2\pi = 116$ MHz and $\omega_0/2\pi = 194$ MHz, respectively. Both a commercial high-temperature probe (Bruker Biospin) and a probe designed for temperatures up to 453 K were employed to measure line shapes and NMR relaxation rates. Typically, the $\pi/2$ pulse lengths ranged from 6 to 9 μs. The measurements were performed at temperatures ranging from 203 K to 450 K; here, a Eurotherm temperature controller in combination with a type T thermocouple was used.

^{7}Li NMR SLR rates $1/T_1 = R_1$ were acquired with the saturation recovery pulse sequence $10 \times \pi/2 - t_d - \pi/2 -$ aquisition (acq.).[9,19] An initial pulse train, consisting of ten $\pi/2$ pulses separated by 80 μs, was used to destroy any longitudinal magnetization M_z prior to recording its temperature and frequency dependent recovery as a function of the delay time t_d. Rotating-frame ^{7}Li NMR SLRϱ rates $1/T_{1\varrho} = R_{1\varrho}$ were recorded with the spin-lock technique, $\pi/2\,p(t_{lock}) -$ acq.[15,16,19,25–28] The corresponding (angular) locking frequency ω_1 was chosen to be as low as possible. Here, $\omega_1/2\pi \approx 10$ kHz was used and the duration of the locking pulse t_{lock} was varied from 100 μs to 100 ms. Note that the recycle delay for the SLRϱ experiments was set to at least $5 \times 1/R_1$ in order to guarantee full longitudinal relaxation between each scan. Both R_1 and $R_{1\varrho}$ were obtained by parameterizing the magnetic transients $M_z(t_d)$ and $M_\varrho(t_{lock})$, respectively, by stretched exponentials (see below): $M_z(t_d) \propto 1 - \exp[-(t/T_1)^\gamma]$ and $M_\varrho(t_{lock}) \propto \exp[-(t_{lock}/T_{1\varrho})^{\gamma_\varrho}]$, respectively.

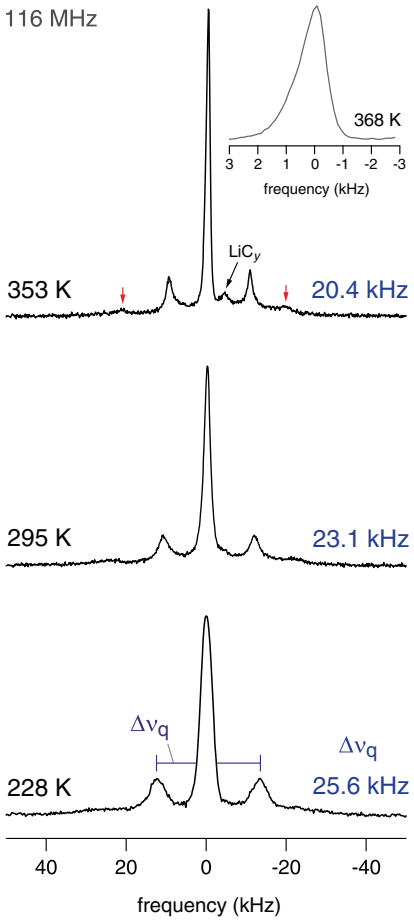

FIG. 2. (Color online) Static ^{7}Li NMR spectra of polycrystalline LiC_6 (116 MHz) recorded at the temperatures indicated. With increasing T homonuclear dipole-dipole interactions are averaged owing to Li^+ hopping which results in narrowing of the linewidths. The quadrupole coupling constant $C_q = 2\Delta\nu_q$ decreases with increasing temperature. The slight anisotropy of the central line (see inset) is due to the layered structure of the sample.

In addition, temperature-variable ^{7}Li NMR spin-spin relaxation (SSR) rates $1/T_2 = R_2$ were recorded by taking advantage of a (two-pulse) solid-echo pulse sequence,[19] that had been optimized for spin-3/2 nuclei such as ^{7}Li. t_{echo} in $\pi/2 - t_{echo} - (64^\circ) -$ acq. denotes the variable interpulse delay. The transients obtained can be satisfactorily described with single exponentials. Static ^{7}Li NMR spectra were either obtained after Fourier transformation (FT) of the free induction decay, which were recorded by nonselective irradiation with a single $\pi/2$ pulse, or by FT of the solid echo beginning from the top of the signal.

III. RESULTS AND DISCUSSION

A. NMR spectra and motional narrowing

Before discussing our SLR NMR results in detail, we call the reader's attention to the static ^{7}Li NMR spectra shown in Fig. 2 which were recorded at different temperatures T. Let us first discuss the central line of the spectrum which is also determined by a distinct powder pattern because of electric

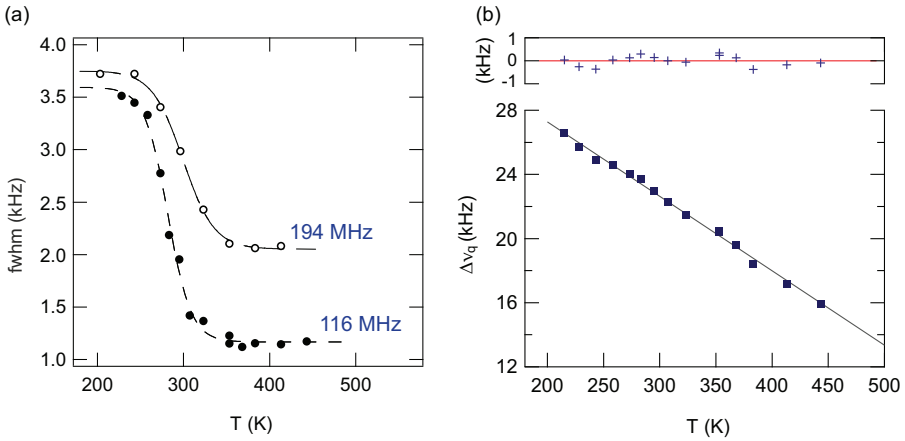

FIG. 3. (Color online) (a) Motional narrowing of the ^{7}Li NMR central line of polycrystalline LiC_6. Linewidths (FWHM, full width at half maximum) were recorded at 116 and 194 MHz. Most likely, the field-dependent final width in the regime of extreme narrowing reflects both the effect of chemical shift anisotropy and, more importantly, the influence of local magnetic field gradients on the spin-spin-relaxation time; see also Ref. 29. (b) Temperature dependence of $\Delta\nu_q$; the upper graph shows the deviations from the linear fit used to describe $\Delta\nu_q(T)$.

quadrupolar interactions (see below). At sufficiently low T, Li^+ translational motion is slow compared to the spectral width determined by the central transition. This results in dipolarly broadened NMR spectra. Motion-induced averaging of dipolar interactions causes line narrowing at elevated T [see Fig. 3(a)]. Expectedly, its overall width (full width at half maximum) in the rigid-lattice regime slightly depends on the strength B_0 of the external magnetic field applied [Fig. 3(a)]. The relatively low, absolute value is compatible with lithium ions lying in planes with six nearest Li neighbors at a distance of approximately 4.3 Å. With increasing T mainly Li-Li dipolar interactions are averaged due to diffusive motion of the spins. From the motional narrowing (MN) curve an activation energy for Li hopping can be roughly estimated with the relation introduced by Waugh and Fedin. Line narrowing sets in at $T_n \approx 260$ K which translates into $E_{a,\,MN}/\text{meV} \approx 1.62 \times T_n/\text{K} \mathrel{\hat{=}} 0.42$ eV. This value is comparable with the one deduced from the low-T flank of the NMR relaxation rate peaks analyzed below; see also Ref. 30. An analysis according to the Abragam formalism[31] yields an even lower activation energy ($\leqslant$0.2 eV). Possible shortcomings of such analyses have recently been outlined in the study of Faske *et al.* and Storek *et al.*[32,33]

At high temperatures the central line reveals a slight anisotropic broadening which reflects the Li ions exposed to the layer structure of LiC_6. Furthermore, in this high-T range, the NMR linewidths of the two-pulse spectra are presumably affected by internal inhomogeneous magnetic fields[29] that arise from the nonzero susceptibility of the LiC_6 particles (see also below, Sec. III B2).

The spectrum recorded at 353 K (see Fig. 2) revealed a small amount of impurities as indicated by the arrow. Fortunately, such a small amount has negligible influence on the SLR NMR rates recorded. The signal with low intensity, that becomes visible at elevated temperatures only, might be ascribed to stage-n graphite intercalation compounds (GICs) such as LiC_{18}, LiC_{27}, or LiC_{36}.[34] These might be formed because of Li loss during preparation. Small amounts of the stage-2 GIC LiC_{12}, as found by XRPD (see above), could hardly be detected by NMR. In particular, LiC_{12} should be distinguishable by its different quadrupole powder pattern characterized by a smaller coupling constant[34] (see also below). Note that the spectra shown in Fig. 2 are plotted such that the central lines show up at $\nu = 0$ kHz. When referenced to an aqueous solution of LiCl (0.1 M), the NMR shift, i.e., the isotropic Knight shift, turns out to be about 41.6 ppm. This is in perfect agreement with results reported and discussed in the literature[14] for LiC_6 (about 42.6 ppm),[34] previously.

Owing to the interaction of the quadrupole moment of ^{7}Li (spin-quantum number 3/2) with a nonvanishing electric field gradient (EFG) at the nuclear site,[31,35,36] the NMR spectra are composed of satellite intensities forming a well-defined quadrupole powder pattern. Since the Li sites are electrically equivalent, a single pattern is observed. From the inner singularities (the outer ones are marked in Fig. 2 by vertically drawn arrows) the site-specific quadrupole coupling constant $C_q = 2\Delta\nu_q$ can be estimated; see the NMR spectrum recorded at 228 K (Fig. 2). Assuming axial symmetry ($\eta = 0$), as expected from the crystal structure, the quadrupole splitting $\Delta\nu_q$ is given by $\Delta\nu_q = |e^2qQ/(2h)|[3\cos^2(\theta) - 1]$ where θ denotes the angle between the c axis and the external magnetic field (in the principal axis system). e is the elemental charge, eq represents the EFG at the Li site, Q is the quadrupole moment of ^{7}Li, and h denotes Planck's constant. At the position of the 90° singularities we obtain $\Delta\nu_q = |e^2qQ/(2h)|$ leading to $2\Delta\nu_q = |e^2qQ/h| = C_q$. This yields 46.2 kHz for the quadrupole coupling constant at 295 K. Note once again that the values given in Fig. 2, and those shown as a function of T in Fig. 3 as well, were obtained for an axially oriented EFG with respect to the principal axis system. The absolute values are consistent with those from ^{7}Li-NMR and ^{8}Li-β-NMR measurements in the literature.[34,37] As an example, Letellier *et al.*[34] found $\Delta\nu_q = 22.6$ kHz at ambient temperature which is in good agreement with our value (23.1 kHz). Using an oriented sample, Roth *et al.*[38] report a value of 22 kHz; in an early work of Conard *et al.*[39] a splitting of 24 kHz is found. LiC_{12}, LiC_{18}, LiC_{27}, and LiC_{36} show smaller quadrupole splittings $\Delta\nu_q$ ranging from 17 to 19 kHz.[34]

It is worth noting that the decrease of the quadrupole splitting $\Delta\nu_q$ with increasing T cannot simply be ascribed to changes of the lattice parameters. Owing to the narrower temperature range covered we were not able to reveal the $T^{3/2}$ dependence found by β-NMR on an oriented LiC_6 sample.[37] Here, $\Delta\nu_q$ (200 K $< T <$ 450 K) changes linearly with T.

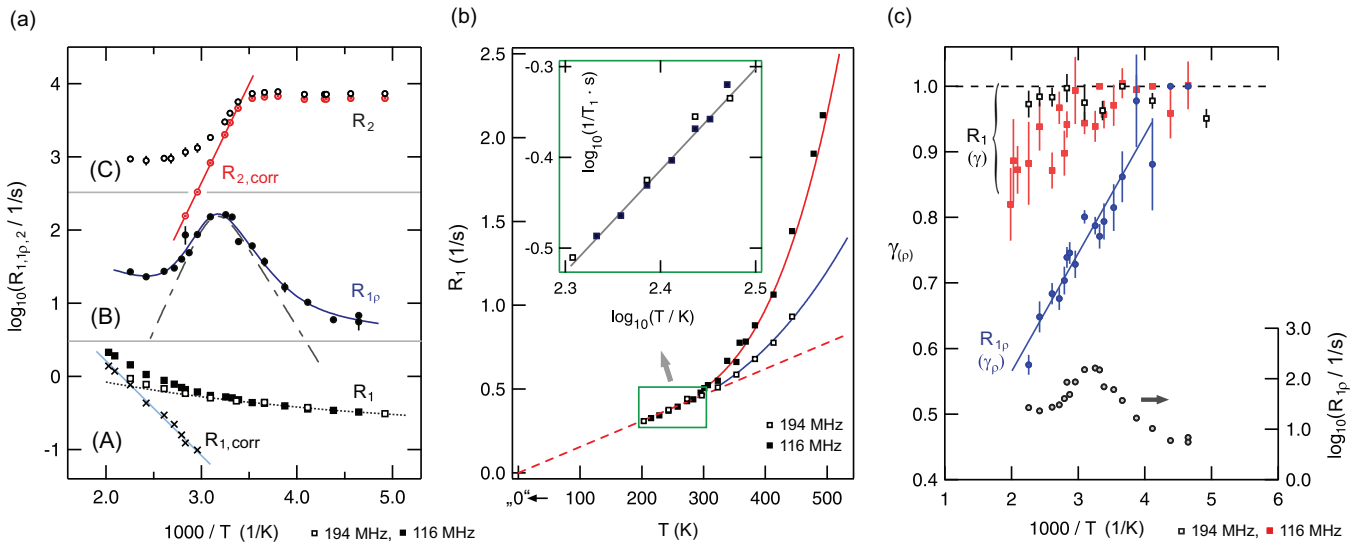

FIG. 4. (Color online) (a) Arrhenius plot illustrating the temperature dependence of the ^{7}Li NMR relaxation rates R_1 (A) and $R_{1\varrho}$ (B) measured at 116 and 194 MHz, respectively; R_2 (C) rates were recorded at 116 MHz. (b) R_1 of LiC_6 plotted as R_1 vs T and $\log_{10} R_1$ vs $\log_{10} T$ (inset). (c) Temperature dependence of the stretching factors γ obtained from the various temperature-variable NMR relaxation transients; exemplarily, selected transients M_ϱ are depicted in Fig. 5(b). For comparison, $R_{1\varrho}(1/T)$ is also shown. See text for further explanations.

B. Diffusion-induced relaxation NMR

1. *^{7}Li SLR NMR in the laboratory and rotating frame of reference*

In the Arrhenius presentation of Fig. 4(a) an overview of the ^{7}Li NMR relaxation rates measured is given. At first we will briefly discuss the SLR NMR rates recorded at 116 MHz and 194 MHz, i.e., in the laboratory frame of reference. At low temperatures R_1 seems to be independent of the Larmor frequency applied. Combined with a linear dependence of R_1 on temperature, this is expected for SLR being mainly induced by coupling of the Li spins with conduction electrons. Indeed, a power-law fit

$$R_1 \propto T^{\kappa}, \tag{1}$$

indicated by the dotted line shown in Fig. 4(a), yields $\kappa = 1.1(1)$. This can be even better illustrated by plotting R_1 vs T: The dashed line in Fig. 4(b) represents ideal linear behavior according to $R_1 = s'T^{\kappa}$ with $\kappa = 1$. The inset uses the representation $\log_{10} R_1$ vs $\log_{10} T$ to calculate κ in the low-temperature regime with a linear fit. The latter yields $s' = 7.9(3) \times 10^{-4}$ s^{-1} K^{-1} and $\kappa = 1.12(4)$ (cf. the power-law analysis shown above). The product T_1T turns out to be approximately 650 ± 15 s · K, which is in very good agreement with the ^{7}Li NMR result reported by Estrade *et al.*[14] (600 ± 120 s · K).

Above 300 K the rates R_1 increasingly deviate from $R_1 = S_0T$ which points to the influence of other relaxation mechanisms owing to Li^+ hopping processes or (anharmonic) lattice vibrations. A two-phonon Raman process would give $R_1 \propto T^2$ at temperatures T larger or similar to the Debye temperature Θ. In order to separate such background effects from diffusion-induced processes, we extrapolated the power-law fit of Fig. 4(a) to higher temperatures and subtracted the rates from the overall ones measured; i.e.,

$$R_{1,\,\mathrm{corr}} = R_1 - R_{1,\,\mathrm{e}} \tag{2}$$

with $R_{1,\,\mathrm{e}} \approx S_0T^{\kappa}$. If we assume that the background-corrected rates obtained are mainly influenced by Li hopping, an activation energy can be roughly estimated. Note that the rates were recorded in the regime $\omega_0\tau \gg 1$; i.e., the activation energy E_{a,T_1} should be characteristic of short-range (or localized) Li motions in LiC_6. These might include translational processes in LiC_6 with a short jump distance.[5] Here, we obtain 0.25(2) eV which is very similar to the result previously estimated from NMR line narrowing.[14]

Ion dynamics proceeding on a longer length scale, however, can only be probed when the so-called high-T flank of the diffusion-induced rate peak is reached. In the present case, this needs very high temperatures. Fortunately, the spin-lock technique can be used which is *per se* sensitive to slower Li motions covering a longer time scale. Therefore, we recorded diffusion-induced SLR NMR rate peaks at frequencies ω_1 on the order of some kHz instead of using ω_0 with values in the MHz range. Doing so, by formally replacing ω_0 with ω_1 the SLR NMR rate peak shifts towards lower temperature so that both the maximum and the high-T flank become accessible. The corresponding rates $R_{1\varrho}$, which have been extracted from the stretched magnetization transients recorded, are shown in Fig. 4(a) as a function of the inverse temperature. At low temperatures, that is, below 250 K, they are increasingly governed by nondiffusive background effects. Note that the ratio $R_{1\varrho}/R_1$ turns out to be approximately 1.5 orders of magnitude. Thus, besides interactions of the Li spins with conduction electrons in the case of R_1 measurements (see above), the low-T $R_{1\varrho}$ rates seem to be influenced by additional processes (see below). For comparison, the corresponding stretching factors of the various transients measured are shown in Fig. 4(c). In Fig. 5 selected magnetization transients of the $R_{1\varrho}$ NMR measurements are shown.

Finally, with increasing T the overall rates $R_{1\varrho}$ pass through a maximum located at $T = 314$ K. At even higher

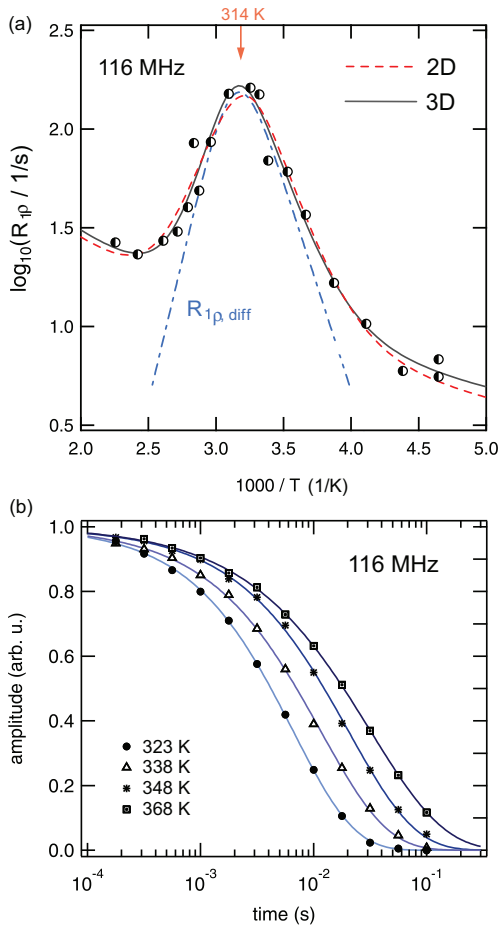

FIG. 5. (Color online) (a) ^{7}Li SLRρ NMR rates of polycrystalline LiC_6 (see Fig. 4), plotted in an Arrhenius diagram. For comparison with the fit according to Eqs. (3) and (4) (solid line), the dashed line represents the 2D fit by means of Eq. (6). The dashed-dotted line shows the purely Li^+ diffusion-induced contribution when the rates are analyzed in terms of a modified BPP-type spectral density function yielding 0.57(2) eV and $\beta = 1.7(2)$. (b) Selected temperature-variable magnetization transients $M_\varrho(t_{\rm lock})$ containing the ^{7}Li SLR NMR rates in the rotating frame of reference. The transients illustrate the behavior of M_ϱ on the high-T flank of the diffusion-induced rate peak shown above. Solid lines show fits with stretched exponentials $M_\varrho(t_{\rm lock}) \propto \exp[-(t_{\rm lock}/T_{1\varrho})^{\gamma_\varrho}]$; in this T range the stretching factor γ_ϱ, also shown in Fig. 4(c), scatters around 0.7 [see Fig. 4(c)].

temperatures, i.e., when $R_{1\varrho}$ decreases, the nondiffusive relaxation background shows up again. In order to separate unwanted background effects from diffusion-induced contributions, the overall rates $R_{1\varrho}$ were, in the first place, approximated with a sum of a modified BPP-type relaxation function and a power-law expression:

$$R_{1\varrho}^{\rm 3D} = R_{1\varrho,\,\rm diff}^{\rm 3D} + R_{1\varrho,\,\rm bgr} = C_\varrho\big(J(2\omega_1) + \tfrac{5}{3}J(\omega_0) + \tfrac{2}{3}J(2\omega_0)\big) + BT^{\kappa'} \quad (3)$$

with $J(\omega_{1(0)})$ being here a Lorentzian-shaped spectral density function according to

$$J(\alpha\cdot\omega_{1(0)})_{\alpha=1,2} = C'\tau_{\rm c}/[1+(\alpha\cdot\omega_{1(0)}\tau_{\rm c})^{\beta}]. \quad (4)$$

Note that the correlation rate $\tau_{\rm c}^{-1}$ is on the order of the jump rate τ^{-1}. In many cases it can be described by an Arrhenius relation containing the pre-exponential factor τ_0^{-1} and the activation energy $E_{\rm a}$ determining long-range Li diffusion

$$\tau_{\rm c}^{-1} \approx \tau^{-1} = \tau_0^{-1}\exp(-E_{\rm a}/k_{\rm B}T); \quad (5)$$

$k_{\rm B}$ denotes Boltzmann's constant. Here, the best fit yields $\kappa' = 2.0(4)$, thus indicating that lattice vibrations become the main origin of background relaxation (see above). The parameter β reflects any asymmetry of the rate peak $R_{1\varrho}(1/T)$ which may arise from correlation effects such as structural disorder and/or Coulomb interactions.[20,21] In general, uncorrelated motion should result in a symmetric NMR rate peak; any correlation effects, for comparison, are expected to reduce the slope on the low-T side compared to the situation in the limit $\omega_1\tau \ll 1$, that is, the high-T regime. In the present case we found $\beta = 1.7(2)$; thus, the diffusion-induced rate peak, indicated by the dashed-dotted line in Fig. 4(a), is slightly asymmetric.

The activation energy $E_{\rm a}$ turned out to be 0.57(2) eV; the prefactor τ_0^{-1} is approximately 1.6×10^{14} s^{-1}. The latter is in very good agreement with values typically expected for phonon frequencies. Moreover, $E_{\rm a} \approx 0.57$ eV is consistent with the prediction of Freiländer *et al.*[7] The value obtained from Eq. (3) also equals the activation energy which can be directly obtained from the high-T side of the rate peak. Moreover, in the limit $\omega_1\tau \gg 1$, where $J(\omega_1,\tau) \propto \omega^{-\beta}\tau^{1-\beta}$ holds, the corresponding slope yields $E_{\rm a,low} = 0.42(2)$ eV. In the present case, $E_{\rm a,low}$ and $E_{\rm a}$ obey the relation $E_{\rm a,low} = (\beta-1)E_{\rm a}$. Note that the same result is obtained when Eq. (3) is restricted to the first term: $R_{1\varrho,\,\rm diff} \propto J(2\omega_1)$.

It is worth noting that $J(\omega)$ in Eq. (4) represents a spectral density function which describes diffusive motion in three dimensions (3D). Frequency-dependent β-NMR measurements,[7,8] however, indicate a low-dimensional diffusion process in LiC_6. Additionally, at temperatures higher than 630 K, a 2D motional process was claimed based on QENS measurements.[5] Therefore, we also tried to analyze our SLR NMR data with a semiempirical spectral density function for 2D diffusion. In concrete terms, we used the expression by Richards[40,41] which is based on a function introduced by Avogadro and Villa taking account of a logarithmic frequency dependence in the high-temperature limit $\omega_{0(1)}\tau_{\rm c} \ll 1$.[42,43] Following Küchler *et al.*,[44] who first incorporated the effect of correlation via the parameter β also for 2D diffusion, it reads

$$R_{1\varrho}^{\rm 2D} = R_{1\varrho,\,\rm diff}^{\rm 2D} + R_{1\varrho,\,\rm bgr} \approx C'_\varrho\tau_{\rm c}\ln[1+1/(2\omega_1\tau_{\rm c})^{\beta}] + B'T^{\kappa''}. \quad (6)$$

This ansatz worked well for other layer-structured materials showing 2D diffusion.[10,12,13,18] The fit, indicated in Fig. 5 by the dashed line, yields $B \approx B'$ and $\kappa' \approx \kappa''$. Moreover, $E_{\rm a}^{\rm 2D}$ is given by approximately 0.62 eV and, thus, at least comparable to the result obtained by Eqs. (3) and (4). However, in the present case, the prefactor τ_0^{-1} turns out to be unusually high; it would be approximately 1.8×10^{16} s^{-1}. This is by about two orders of magnitude larger than that obtained from the modified-BPP fit used to describe the temperature dependence of the NMR rates (*vide supra*). Hence, based on the results obtained it seems that the semiempirical Richards model (represented by the dashed line in Fig. 5) is less appropriate to

describe Li dynamics in LiC_6. Certainly, this fact might also be explained by nonnegligible Li hopping processes taking place via defects perpendicular to the layers, that is, channel-like diffusion, influencing the NMR response of a pure 2D process.

2. ^{7}*Li NMR spin-spin relaxation*

The results obtained from SLR NMR are corroborated by the analysis of complementary spin-spin relaxation (SSR) data. In agreement with the results of Eqs. (3) and (4), temperature-variable SSR measurement yield an activation energy of 0.53(2) eV. This value can be extracted from the rates measured as follows. Below 285 K, that is, in the so-called rigid lattice regime, R_2^{-1} is almost independent of temperature and amounts to approximately 125 μs. Owing to averaging of dipole-dipole interactions, because of increasing of the Li^+ hopping, the rates significantly start to decrease indicating long-range Li translational motion. Interestingly, at 400 K they reach a plateau value characterized by $R_{2,\mathrm{high}}^{-1} \approx 1$ ms. This feature is very similar to the one observed by McDowell *et al.*[29] previously in the 2D H^+ ion conductor $ZrBe_2H_{1.4}$ (ZBH). In ZBH the deviation is ascribed to long-range H motion in the presence of a magnetic field gradient which is due to the nonzero magnetic susceptibility of the metal hydride. The mean-field gradient in ZBH is directly proportional to the magnitude B_0 of the external magnetic field applied. As a result, the lower the Larmor frequency used the farther the beginning of the plateau is shifted towards higher temperature resulting in a decrease of $R_{2,\mathrm{high}}$. Hence, the residual NMR (central) linewidth in the regime of extreme motional narrowing is expected to be smaller for measurements carried out at 116 MHz compared to those performed at 194 MHz [see Fig. 3(a)].

Subtracting $R_{2,\mathrm{high}}$ from the overall rates measured yields $R_{2,\mathrm{corr}}$. From the linear fit shown in Fig. 4(a) the above-mentioned activation energy [0.53(2) eV] can be deduced. Lastly, with the help of both $R_{1\varrho}$ and R_2 measurements it is possible to probe Li diffusion in LiC_6 at temperatures ranging from 270 K to 360 K. This regime coincides with the operating range for most battery applications.

C. Li jump rates and self-diffusion coefficients

Considering the maximum of the $R_{1\varrho}(1/T)$ peak probed, it is possible to precisely determine the mean Li jump rate irrespective of the spectral density function J chosen to parametrize the data. At $T = 314$ K, that is the temperature where the peak shows up [see Fig. 5(a)], for SLR NMR in the rotating frame of reference the condition $\omega_1\tau_c \approx 0.5$ holds.[9] Identifying τ_c with the motional residence time of an Li spin and inserting $\omega_1 = 2\pi \times 10(1)$ kHz, we obtain $\tau_c \approx \tau = 8$ μs. According to the Einstein-Smoluchowki equation,[46]

$$D_{d\mathrm{D}} = a^2/(2d \cdot \tau), \tag{7}$$

this corresponds to $D_{2\mathrm{D}}(314\mathrm{K}) \approx 1.9 \times 10^{-11}$ cm^2 s^{-1} and $D_{3\mathrm{D}}(314\ \mathrm{K}) \approx 1.3 \times 10^{-11}$ cm^2 s^{-1}. Here, we used $a \approx 3$ Å as a good approximation for a mean jump distance and calculated the diffusion coefficient for both spatially restricted and nonrestricted motion, i.e., for $d = 2$ or $d = 3$, whereby d represents the dimensionality of the diffusion process.

In Fig. 6(a) the jump rate determined by means of the Li^+ diffusion-induced $R_{1\varrho}(1/T)$ rate peak is shown in an Arrhenius plot and compared with those values which can be estimated from (analogous) ^{8}Li β-NMR measurements of Freiländer *et al.*[7] Although ^{8}Li NMR was carried out on oriented (HOPG) LiC_6 samples good agreement is found. For comparison, the solid line represents an Arrhenius line characterized by an activation energy of 0.55 eV, which represents the mean value when the results from $R_{1\varrho}$ and R_2 are considered. The gray area indicates the temperature range covered by Li^+ diffusion-induced $R_{1\varrho}$ measurements. From the Arrhenius line indicated a prefactor τ_0^{-1} can be estimated ($\approx 1 \times 10^{14}$ s^{-1}) which is consistent with that obtained from the analysis of the $R_{1\varrho}(1/T)$ NMR peak with a BPP-type expression (*vide supra*).

Besides $R_{1\varrho}$ measurements also R_2 (and motional line narrowing as well) is suitable to estimate Li jump rates. At the temperature where the rates R_2 start to decrease [$T \approx 294$ K; see Fig. 4(a)] the Li jump rate is expected to be on the order of $\tau^{-1} \approx 2\pi R_{20}$ with $R_{20}^{-1} = T_{20} = 140$ μs being the rigid-lattice SLR NMR rate. This yields $\tau = 22$ μs. Even slower motions can be estimated from the onset of motional line narrowing; in the present case NMR central lines significantly start to decrease in linewidth at $T \approx 250$ K. Roughly spoken, this is expected when τ reaches values on the order of a few ms. Additionally, the inflexion point ($T_{\mathrm{infl.}} \approx 275$ K at 116 MHz) of the whole motional narrowing (MN) curve (see above, Fig. 3) can be used to estimate τ according to $\tau^{-1}(T_{\mathrm{infl.}}) \approx 2\pi\nu_0$ with ν_0 being the rigid-lattice linewidth ($\approx$3.5 kHz). For comparison, the values estimated from SSR NMR and MN are also included in Fig. 6(a).

It is worth noting that in the presence of a broad distribution of jump rates [note that such a feature would also be reflected in a deviation of β from BPP-type behavior ($\beta = 2$)], the NMR line narrowing would be predominantly influenced by that fraction of ions diffusing faster compared to others. Hence, as indicated above, the interpretation of MN NMR data can easily lead to an overestimation of the mean lithium jump rate and an underestimation of the activation energy; see, e.g., Refs. 32 and 33. For comparison, activation barriers ranging from 0.1 and 0.3 eV have been calculated for different types of interstitialcy diffusion mechanisms in LiC_6.[22]

Finally, considering the rates shown in Fig. 6(a), at room temperature (293 K) the Li jump rate turns out to be 4.5×10^4 s^{-1}. This corresponds to a self-diffusion coefficient on the order of 5×10^{-12} cm^2 s^{-1} at 293 K. Decreasing the temperature from 293 to 268 K (−5 °C), Li self-diffusivity is slowed down by a factor of 10. Such key figures are crucial for the safe and efficient operation of graphite-based ion batteries. In particular, at freezing temperatures the performance of a battery is then additionally limited and controlled to a large extent by slow Li diffusion within the host material. It is noteworthy that room-temperature self-diffusion coefficients ranging from 10^{-16} m^2 s^{-1} to 10^{-15} m^2 s^{-1}, as found for LiC_6 here, are comparable to those recently obtained by NMR also for layer-structured cathode materials such as $Li_{x\approx 0.7}TiS_2$.[10] Thus, regarding Li *self-diffusion* in fully intercalated stage-1 LiC_6, Li ion mobility does not exceed that of conventional cathode materials.

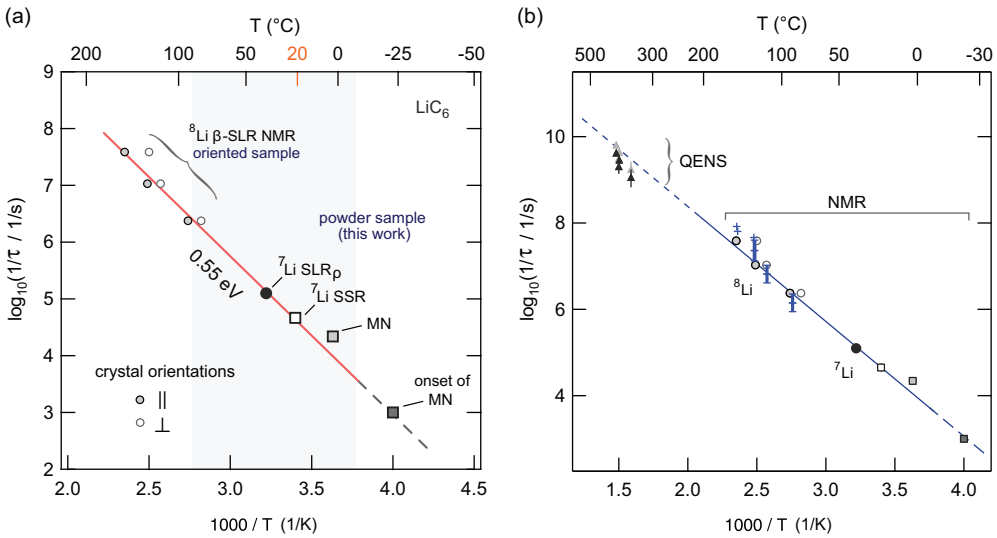

FIG. 6. (Color online) (a) Arrhenius plot of Li jump rates in LiC_6 deduced from various NMR techniques being sensitive to translational ion jumps on quite different time scales, here, covering up to five decades. SLR NMR rate peaks provide a relatively theory-independent determination of jump rates. The rates determined by β-NMR were deduced from Ref. 7. See text for further explanation. (b) Comparison of the rates shown in (a) with those obtained from QENS (Ref. 5). The diffusion coefficients from QENS reported by Magerl *et al.* (Ref. 5) have been roughly converted into jump rates τ^{-1} (triangles in black) via the Einstein-Smoluchowski equation [see Eq. (7)] assuming, as suggested in Ref. 5, 2D diffusion and a relatively long jump distance a of approximately 4.26 Å. Using $a \approx 3$ Å, which is close to the average of possible jump distances in LiC_6, yields the rates shown by gray triangles. $a = 2.5$ Å, which is the jump distance for an interstitial migration mechanism (Refs. 22 and 45), yields an even better agreement. The crosses represent jump rates from β-NMR presented in Ref. 8.

Strictly speaking, the results presented here should not be mixed with *chemical* diffusion coefficients which have been experimentally probed via (solid-state) electrochemical macroscopic method as well as calculated (4×10^{-12} m^2 s^{-1}, $E_a \approx 0.4$ eV) recently for 2D (in-plane) Li^+ motion in LiC_6.[47] Interestingly, the results of the theoretical work by Toyoura *et al.*[45] on ordered LiC_6 agree well with the present findings. Activation barriers for Li migration, which were calculated separately for the vacancy and interstitial Li migration process, turned out to be approximately 0.5 eV; see also Ref. 22. The corresponding (in-plane) diffusion coefficients are 10^{-14} m^2 s^{-1} and 10^{-15} m^2 s^{-1}, respectively. Apart from this good agreement, the present results are in line with those from earlier experimental studies; see, e.g., Ref. 48 for an overview of Li (chemical) diffusion coefficients determined for various carbon anode materials. Note that by the application of NMR spectroscopy we were able to study Li ion dynamics separately from electron dynamics in mixed conducting LiC_6. While the latter influences the SLR NMR rates recorded at low temperatures, with increasing T diffusive motions significantly govern spin-lattice relaxation while other interactions relatively lose ground. These show up once again at temperatures higher than 400 K.

As a last comparison, in Fig. 6(b) data from the QENS study of Magerl *et al.*,[5] pointing to an in-plane 2D jump-type diffusion mechanism, are included. The self-diffusion coefficients deduced from QENS have been roughly converted into jump rates according to Eq. (7). Here, we used both $a \approx 4.26$ Å as found by QENS for the 2D diffusion process and $a \approx 3$ Å, which is a good approximation for the average of possible jump distances. Considering the error limits and the narrow temperature range covered by the earlier study,[5] in our opinion, a relatively good agreement is found with the results obtained from NMR. The solid line is to guide the eye and refers to an Arrhenius law with $E_a = 0.54$ eV and $\tau_0^{-1} = 5 \times 10^{13}$ s^{-1} which is very similar to that shown in Fig. 6(a). To sum up, over a relatively broad dynamic range a single Arrhenius relation seems to be appropriate to describe Li diffusion in ordered LiC_6.

IV. CONCLUSIONS AND OUTLOOK

Spin-lattice relaxation NMR using the stable isotope ^{7}Li was applied to probe room-temperature Li dynamic parameters in polycrystalline, mixed conducting LiC_6 being the most widely used anode material. As deduced from atomic-scale NMR measurements Li hopping in the bulk is characterized by an activation energy of approximately 0.55 eV and an Li self-diffusion coefficient of 10^{-15} m^2 s^{-1} (295 K), thus, comparable to Li self-diffusivity in layer-structured transition metal sulfides and oxides serving as positive electrodes in lithium-ion batteries.

The results obtained from the different NMR techniques employed are in good agreement with previous studies[7,8] using ^{8}Li β-NMR to probe diffusion parameters at elevated temperatures. Most importantly, the jump rates can be well approximated with a *single* Arrhenius law which is determined by an activation energy of approximately 0.55 eV and a pre-factor on the order of typical phonon frequencies, viz., 10^{14} s^{-1}. On that note the present study updates our knowledge on Li self-diffusion in LiC_6. It is noteworthy that the activation energy probed by NMR is in fair agreement with calculated barrier heights ($\approx$0.5 eV) by Toyoura *et al.*[45] for both the in-plane vacancy and interstitial Li migration mechanism. Even the

chemical diffusion coefficients reported by Toyoura *et al.*[45] (viz., 10^{-14} m^2 s^{-1} and 10^{-15} m^2 s^{-1} for the interstitial and vacancy mechanism, respectively) agree with the present findings.

Considering solely ^{7}Li NMR rates, it is difficult to judge whether the diffusion process probed is strictly governed by 2D diffusion. The present results are in very good agreement with those probed by orientation-dependent and frequency-dependent SLR ^{8}Li β-NMR measurements on highly oriented pyrolytic graphite. The β-NMR results indeed gave strong evidence for low-dimensional lithium diffusion.[7,8] Fair agreement is also found with results from QENS probing in-plane diffusion in the ordered phase of LiC_6.[5] Recent theoretical investigations also strongly point to high lithium-ion diffusivity in the direction parallel to the graphene layers and to much slower interlayer hopping, that is, motion across the basal plane.[47]

However, though there are convincing reasons to claim even microscopic Li diffusion as purely low-dimensional in LiC_6, the semiempirical SLR NMR model introduced by Richards for 2D motion seem to be less adequate to satisfactorily describe the temperature dependence of the ^{7}Li NMR $R_{1\varrho}(1/T)$ rate peak probed here. The applicability of a modified BPP-type relaxation model, see, e.g., the previous work by Küchler *et al.*,[44] might indicate a small, but nonnegligible, influence of interlayer hopping process on the diffusion-induced SLR NMR rates.

To shed further light on the Li dynamics in LiC_6, the application of NMR techniques being able to directly record motional correlation functions might be beneficial. For instance, considering the temperature range below 300 K, this should be possible via the generation of Jeener-Broekaert NMR echoes[49] with the so-called spin-alignment echo (SAE) technique.[50–53] In general, SAE (or stimulated echo) NMR is sensitive to extremely slow translational and rotational jump processes.[54–60]

ACKNOWLEDGMENTS

We thank our colleagues at the TU Graz and at the Leibniz University Hannover for valuable discussions. Financial support by the Deutsche Forschungsgemeinschaft (DFG) is highly appreciated (DFG Research Unit 1277, Grant No. WI3600/2-2 and 4-1 and Grant No. HE1574/13-2), and by the Austrian Federal Ministry of Economy, Family, and Youth and the Austrian National Foundation for Research, Technology, and Development is greatly appreciated.

*The authors were equally involved in experimental work, data analysis, and project planning. Corresponding author: julia.langer@tugraz.at

†See also for correspondence: viktor.epp@tugraz.at

‡See also for correspondence: wilkening@tugraz.at

[1] M. S. Whittingham, Chem. Rev. **104**, 4271 (2004).

[2] J. M. Tarascon and M. Armand, Nature (London) **414**, 359 (2001).

[3] M. Wakihara and O. Yamamoto, eds., *Lithium Ion Batteries* (Wiley-VCH, Weinheim, 1998).

[4] M. Winter and J. O. Besenhard, Electrochem. Acta **45**, 31 (1999).

[5] A. Magerl, H. Zabel, and I. S. Anderson, Phys. Rev. Lett. **55**, 222 (1985).

[6] T. Springer and R. E. Lechner, in *Diffusion in Condensed Matter—Methods, Materials, Models*, 2nd ed, edited by P. Heitjans and J. Kärger (Springer, Berlin, 2005), Chap. 3, pp. 91–164.

[7] P. Freiländer, P. Heitjans, H. Ackermann, B. Bader, G. Kiese, A. Schirmer, H.-J. Stöckmann, C. V. der Marel, A. Magerl, and H. Zabel, Z. Phys. Chem. **151**, 93 (1987).

[8] A. Schirmer and P. Heitjans, Z. Naturforsch. **50a**, 643 (1995).

[9] P. Heitjans, A. Schirmer, and S. Indris, in *Diffusion in Condensed Matter*, edited by P. Heitjans and J. Kärger (Springer, Berlin, 2005), Chap. 9, p. 367.

[10] M. Wilkening and P. Heitjans, Phys. Rev. B **77**, 024311 (2008).

[11] M. Wilkening, A. Kuhn, and P. Heitjans, Phys. Rev. B **78**, 054303 (2008).

[12] V. Epp and M. Wilkening, Phys. Rev. B **82**, 020301 (2010).

[13] V. Epp, O. Gün, H.-J. Deiseroth, and M. Wilkening, Phys. Chem. Chem. Phys. **15**, 7123 (2013).

[14] H. Estrade, J. Conard, P. Lauginie, P. Heitjans, F. Fujara, W. Buttler, G. Kiese, H. Ackermann, and D. Guérard, Physica B **99**, 531 (1980).

[15] D. Ailion and C. P. Slichter, Phys. Rev. Lett. **12**, 168 (1964).

[16] C. P. Slichter and D. Ailion, Phys. Rev. **135**, A1099 (1964).

[17] M. Wilkening, W. Iwaniak, J. Heine, V. Epp, A. Kleinert, M. Behrens, G. Nuspl, W. Bensch, and P. Heitjans, Phys. Chem. Chem. Phys. **9**, 6199 (2007).

[18] V. Epp, S. Nakhal, M. Lerch, and M. Wilkening, J. Phys.: Condens. Matter **25**, 195402 (2013).

[19] E. Fukushima and S. B. W. Roeder, *Experimental Pulse NMR: A Nuts and Bolts Approach* (Addison-Wesley Pub. Co., Advanced Book Program, Reading, MA, 1981).

[20] M. Meyer, P. Maass, and A. Bunde, Phys. Rev. Lett. **71**, 573 (1993).

[21] A. Bunde, W. Dieterich, P. Maass, and M. Meyer, in *Diffusion in Condensed Matter—Methods, Materials, Models*, 2nd ed, edited by P. Heitjans and J. Kärger (Springer, Berlin, 2005), Chap. 20, pp. 813–856.

[22] K. Toyoura, Y. Koyama, A. Kuwabara, and I. Tanaka, J. Phys. Chem. C **114**, 2375 (2010).

[23] A. Herold, Synth. Met. **23**, 27 (1988).

[24] D. Guérard and A. Hérold, Carbon **13**, 337 (1975).

[25] D. C. Ailion and C. P. Slichter, Phys. Rev. **137**, A235 (1965).

[26] D. C. Look and I. J. Lowe, J. Chem. Phys. **44**, 2995 (1966).

[27] T. J. Rowland and F. Y. Fradin, Phys. Rev. **182**, 760 (1969).

[28] D. Wolf, Phys. Rev. B **10**, 2724 (1974).

[29] A. F. McDowell, C. F. Mendelsohn, M. S. Conradi, R. C. Bowman, and A. J. Maeland, Phys. Rev. B **51**, 6336 (1995).

[30] M. Wilkening, D. Bork, S. Indris, and P. Heitjans, Phys. Chem. Chem. Phys. **4**, 3246 (2002).

[31] A. Abragam, *The Principles of Nuclear Magnetism* (Clarendon, Oxford, 1961).

[32] S. Faske, H. Eckert, and M. Vogel, Phys. Rev. B **77**, 104301 (2008).

[33]M. Storek, R. Böhmer, S. W. Martin, D. Larink, and H. Eckert, J. Chem. Phys. **137**, 124507 (2012).
[34]M. Letellier, F. Chevallier, and F. Béguin, J. Phys. Chem. Solids **67**, 1228 (2006).
[35]P. Diehl, E. Fluck, H. Günther, R. Kosfeld, and J. Seelig, eds., *NMR—Basic Principles and Progress*, Vol. 30 (Springer, Berlin, 1994).
[36]D. Freude and J. Haase, in *NMR–Basic Principles and Progress*, edited by P. Barker and H. Pfeiffer, Vol. 29 (Springer, Berlin, 1993).
[37]P. Freiländer, P. Heitjans, H. Ackermann, B. Bader, G. Kiese, A. Schirmer, and H.-J. Stöckmann, Z. Naturforsch. A **41**, 109 (1986).
[38]G. Roth, K. Lüders, P. Pfluger, and H.-J. Güntherodt, Solid State Commun. **39**, 423 (1981).
[39]J. Conard and H. Estrade, Mat. Sci. Eng. **31**, 173 (1977).
[40]P. M. Richards, Solid State Commun. **25**, 1019 (1978).
[41]P. M. Richards, in *Topics in Current Physics*, edited by M. B. Salamon, Vol. 15 (Springer, Berlin, 1979).
[42]A. Avogadro and M. Villa, J. Chem. Phys. **66**, 2359 (1977).
[43]C. A. Sholl, J. Phys. C **14**, 447 (1981).
[44]W. Küchler, P. Heitjans, A. Payer, and R. Schöllhorn, Solid State Ion. **70/71**, 434 (1994).
[45]K. Toyoura, Y. Koyama, A. Kuwabara, F. Oba, and I. Tanaka, Phys. Rev. B **78**, 214303 (2008).
[46]H. Mehrer, *Diffusion in Solids* (Springer, Berlin, 2006).
[47]K. Persson, V. A. Sethuraman, L. J. Hardwick, Y. Hinuma, Y. S. Meng, A. van der Ven, V. Srinivasan, R. Kostecki, and G. Ceder, J. Phys. Chem. Lett. **1**, 1176 (2010).
[48]M. Park, X. Zhang, M. Chung, G. B. Less, and A. M. Sastry, J. Power Sources **195**, 7904 (2010).
[49]J. Jeener and P. Broekaert, Phys. Rev. **157**, 232 (1967).
[50]R. Böhmer, T. Jörg, F. Qi, and A. Titze, Chem. Phys. Lett. **316**, 419 (2000).
[51]F. Qi, T. Jörg, and R. Böhmer, Solid State Nucl. Magn. Res. **22**, 484 (2002).
[52]M. Wilkening, J. Heine, C. Lyness, A. R. Armstrong, and P. G. Bruce, Phys. Rev. B **80**, 064302 (2009).
[53]M. Wilkening, W. Küchler, and P. Heitjans, Phys. Rev. Lett. **97**, 065901 (2006).
[54]X.-P. Tang, R. Busch, W. L. Johnson, and Y. Wu, Phys. Rev. Lett. **81**, 5358 (1998).
[55]M. Lausch and H. W. Spiess, J. Magn. Reson. **54**, 466 (1983).
[56]H. W. Spiess, J. Chem. Phys. **72**, 6755 (1980).
[57]G. Fleischer and F. Fujara, in *NMR—Basic Principles and Progress*, edited by P. Diehl, E. Fluck, H. Günther, R. Kosfeld, and J. Seelig, Vol. 30 (Springer, Berlin, 1994).
[58]F. Fujara, S. Wefing, and H. Spiess, J. Chem. Phys. **84**, 4579 (1986).
[59]T. Dries, F. Fujara, M. Kiebel, E. Rössler,, and H. Silescu, J. Chem. Phys. **88**, 2139 (1988).
[60]M. Wilkening and P. Heitjans, Solid State Ion. **177**, 3031 (2006).